ULTRASONIC IMAGING **18,** 122–139 (1996)
ARTICLE NO. 0007

Phase Insensitive Homomorphic Image Processing for Speckle Reduction

YAN CHEN, SHIRA L. BROSCHAT, AND PATRICK J. FLYNN

School of Electrical Engineering and Computer Science, Washington State University, Pullman, Washington 99164-2752

Speckle appears in all conventional ultrasound images and is caused by the use of a phase-sensitive transducer. Speckle is an undesirable property as it can mask small but perhaps diagnostically significant image features. In this paper a homomorphic, hybrid nonlinear processing method, based on cancellation of scattering interference, is developed and examined. Experiments with synthetic and real ultrasound imagery show that the proposed method improves the contrast-to-noise ratio in both lesion and cyst areas and preserves edge clarity.
KEY WORDS: B-mode ultrasound image; computer model; simulation; speckle reduction.

1. INTRODUCTION

The phenomenon of speckle in ultrasound imaging results directly from the use of a phase-sensitive transducer and occurs when structure in the object is on a scale too small to be resolved by the imaging system [1]. It is an interference phenomenon—small scatterers cause constructive and destructive phase interference at the receiving array. Speckle is an undesirable property as it can mask small but perhaps diagnostically significant image features.

The statistical properties of random walks have been studied for many years [2–4], and their relevance to speckle has been recognized for more than two decades. If there are a large number of scatterers (5 or more according to Tuthill et al. [5]) within a pulse interval, scattering from each scatterer is independent of the others and the phase associated with each of the complex contributions is entirely random, i.e., uniformly distributed over the primary interval [6]. Thus, the speckle amplitude will have a Rayleigh distribution, will remain constant over time for a given transducer and view, and will be mostly dependent on the transducer's characteristics.

Speckle can be reduced by adding images of the same region obtained from transducers using different frequencies and different spatial locations [1–9]. These approaches are called *frequency compounding* and *spatial compounding*, respectively . Frequency compounding [10] has been implemented by dividing a wide bandwidth signal into many bands and summing components or by imaging at several different transducer frequencies. Spatial compounding has been implemented using images of the same region formed with different portions of a phased array. However, the division of the spectrum into different bands or the division of a transducer into different apertures is limited by the resolution,

0161-7346/96 $18.00

frequency response, and size of the transducer. An alternative spatial compounding method has been implemented using lateral aperture translation of the transducer [11]. In this method speckle noise is reduced by summing several correlated images obtained at a series of positions.

Recently, two different approaches have been proposed for speckle reduction, namely *postformation image filtering techniques* and *incoherent processing techniques* [13–18]. These methods are becoming viable largely because of the increasing power of digital signal processing (DSP) chips. Much interest has focused on postformation image filtering. Several adaptive filters have been designed for feature detection in ultrasonic images [11–14]. Most of these techniques utilize variations of the statistical properties of the data samples, observed through a fixed-size moving window, to obtain the output of the filter. The difficulties in implementing such techniques are related to determination of the proper weighting coefficients for the filter and design of an appropriately sized moving window.

Median filtering, a simple postformation filtering technique, is effective for speckle reduction. It chooses the median of the running window as the pixel value and so eliminates any impulse with a duration of less than half the window size. Since the degree of smoothing performed by the median filter is influenced only by the window size, some high frequency signals are also removed during speckle filtering, causing edge blurring. Furthermore, when the speckle size is larger than half the window size, it remains in an image as an artifact.

The adaptive weighted median filter (AWMF) [12] is an improved median filter which eliminates the traditional requirement that the speckle artifact be smaller than half the window size. The weighted median of a window pixel sequence is defined as the median of the extended sequence formed by replicating each pixel intensity $x_{i,j}$, $w_{i,j}$ times, where $w_{i,j}$ are the corresponding integer-valued weights that depend both on the distance between the pixel and the window's central pixel and the local image homogeneity. The filter coefficients are adjusted using image data. This technique is straightforward to implement and constitutes an integral part of the filtering process.

A few researchers have studied incoherent imaging systems [17,18] for which a nonlinear function acts on all outputs of the array elements. The original phase relationships are destroyed even though the same electrical delays are maintained for ultrasound focusing. Because there is no linear summation of element outputs, speckle formation is prevented. Power compression is a simple example of this operation. It uses the root-power relationship to distort the phase relationship of element outputs, and the power index affects each element phase. Imaging with phase-distorted element outputs is different from imaging with a phased array. Thus, we refer to the use of phase-distorted element outputs for imaging as *phase insensitive imaging*. One advantage of the technique is its ability to suppress speckle noise during image formation. With today's rapidly developing DSP hardware, this approach offers the potential for fast, economical speckle reduction.

In this paper, we propose a hybrid phase-insensitive homomorphic processing technique for speckle reduction. Initially, several subimages are formed using separate portions of the transducer, then a log transform is applied to each subimage to destroy the phase relationship between the transducer element outputs. A low frequency emphasis filter is used to smooth high frequency components, and finally an exponential function is applied to recover the original signal level. This hybrid technique has the advantages of incoherent imaging, and it is better than the simple power compression approach because of its

nonlinear and smoothing properties. Experiments with both real and synthetic images show that the method improves the contrast-to-noise ratio in both lesion and cyst areas and preserves edges well.

In Section 2, we describe the phase insensitive imaging technique and introduce our new hybrid approach. Section 3 gives the details of our ultrasound imaging simulations. In sections 4, 5, and 6, we present the simulated image results for various methods, compare their performance, and explain the parameter choices for our proposed method. The test results for a real image are provided in section 7, and conclusions are given in section 8.

2. PHASE INSENSITIVE IMAGING AND HYBRID HOMOMORPHIC METHOD

In this section, we introduce the principle of ultrasound imaging and the speckle formation mechanism. This is followed by a discussion of the phase insensitive imaging technique and an explanation of our approach to speckle reduction.

Figure 1 illustrates image formation in a phase sensitive system. For a single imaging line l perpendicular to the transducer face, the time delays of array elements are controlled such that the transmitted signals from the individual elements reach a particular point at the same time. For transmission (the ultrasound beam focuses at a specified depth z_f), the time delay τ_{il} of the i^{th} element is given by

$$\tau_{il} = \frac{z_f - \sqrt{(x_i - x_l)^2 + z_f^2}}{c}. \tag{1}$$

For a dynamic focusing receiver

$$\tau_{il} = \frac{z_t - \sqrt{(x_i - x_l)^2 + z_t^2}}{c}, \tag{2}$$

where $z_t = ct/2$, c is the sound speed in tissue, t is the time, x_i is the position of the i^{th} element, and x_l is the imaging line location. The left-hand side of figure 1 shows the time delays that compensate for the extra travel time required from each element to A relative to the element located at the imaging line l. The beam produced in this way exploits the phase coherence from element to element along the array. However, because of the phase

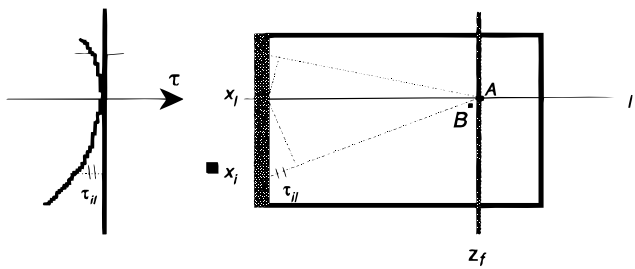

FIG. 1. Illustration of the relationship between time delay and beamforming.

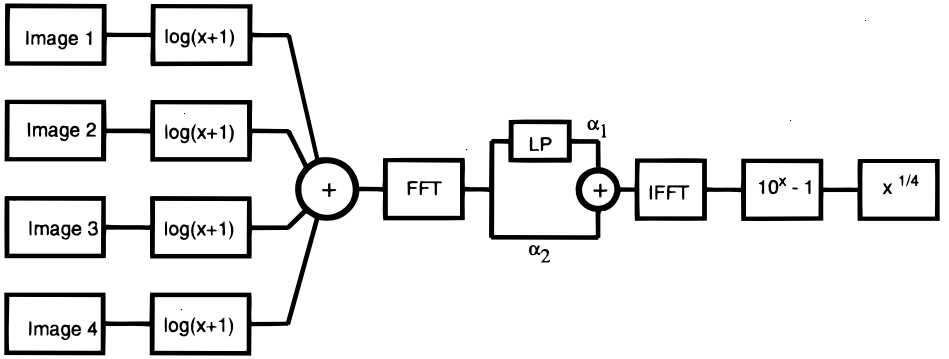

FIG. 2. Diagram of homomorphic algorithm.

sensitivity and pulse duration, a close point *B* is insonified at almost the same time and will affect the image pixel value at position *A*. Most body tissue that is homogeneous within a region contains many randomly arranged scatterers in the sensor's field of view; these scatterers cause constructive and destructive interference, resulting in granular structure (speckle) in an ultrasound image. This interference is difficult to prevent when employing phase sensitive imaging.

Phase insensitive imaging is an improved technique that processes each sensing element value individually. The nonlinear processing of each element's output prior to summation can reduce speckle noise by disrupting phase interference. In power compression (a simple phase insensitive imaging technique), the signal return from each sensing element is compressed, the compressed values are summed across the elements, and the resulting sum is decompressed. The phase relationship between elements is thus destroyed, but the signal retains the same scale. The power compression method yields the following output $B_l(t)$ in terms of the element outputs $E_{jl}(t)$:

$$B_l(t) = \left[\sum_{j=1}^{N} (E_{jl}(t - \tau_{jl}))^{1/q} \right]^q \tag{3}$$

where l is the imaging line, E_{jl} is the j^{th} element output, and τ_{jl} is its associated time delay.

One problem with the phase insensitive technique is that it requires memory, space, and time to record all element outputs (64 or 128 elements in a linear array). An image with 300 $\times$ 300 pixels with gray levels stored at 8 bits/pixel requires about 0.1 MB memory; the 64 subimages needed to form an image consume 6.4 MB. If the sample frequency is 10 MHz (the minimum requirement for a 5 MHz transducer), 64 channels will acquire data simultaneously at a sampling interval of 0.1 μs. It is expensive to achieve these sustained data rates with current DSPs.

To reduce this computational burden, we introduce a hybrid method that combines the phase insensitive technique with a phase sensitive speckle reduction method (either spatial compounding or frequency compounding). We first form several correlated images by summation of subsets of array elements or of some frequency zones. Then we apply nonlinear homomorphic processing to destroy the phase relationship in these images.

Figure 2 shows a flowchart of the proposed method. The input is a set of correlated

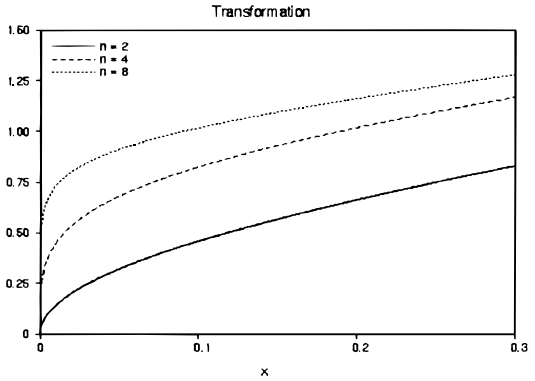

FIG. 3. Transformation function.

subimages (e.g., 4 images) that are log-transformed and summed pixel by pixel. A Fourier transform of the subimages is followed by low pass filtering in the frequency domain and an inverse Fourier transform is performed on the result. The dynamic range is increased in the $10^x - 1$ block, compensating for the earlier log transform. In the final block, the signal is recovered by taking the exponential root ($1/n$ where n is the number of subimages).

With this method, four factors contribute to speckle reduction:

1. The summation of log-transformed images is equivalent to multiplication of the subimages. If the subimages exhibit low pairwise correlation, the subimages have different speckle patterns, and multiplication will decrease the speckle noise greatly. However, the pairwise subimage correlation must not be too small because the multiplication of decorrelated images will then weaken the response from diagnostically significant features (e.g., cysts).

2. Speckle is caused by small tissue scatterers. In the frequency domain, speckle appears as high frequency components relative to the frequency components of lesions, cysts and the incident signal. A smooth low frequency emphasis filter is used to suppress the high frequency components due to speckle.

3. The constants α_1 and α_2 for the low frequency emphasis filter change the log-transformed values exponentially. When $\alpha_1 \cdot L(f) + \alpha_2 > 1$ ($L(f)$ is the low pass filter function), the pixel values are amplified, compensating for the decay due to decorrelated image multiplication.

4. To reduce calculation errors involving small signal magnitudes, we take the logarithm of $x + 1$ instead of x. In the inverse blocks, $10^x - 1$ and the n^{th} root (where n is the number of subimages) are used to compensate for the signal level. This nonlinear method produces an output signal with an enhanced contrast-to-noise ratio. For example, if we set $\alpha_1 = 0$, $\alpha_2 = 1$ and supply identical images to the different channel inputs, the output is $\hat{x} = [(x + 1)^n - 1]^{1/n}$. Figure 3 shows the transformation functions. The dynamic range decreases with increasing n, especially for small values of x, thus reducing the output noise variance.

We can obtain correlated subimages using spatial or frequency compounding. For spatial subimage formation, we sum the odd and even element outputs separately and obtain two subimages. The correlation coefficient decreases with an increase in the distance between

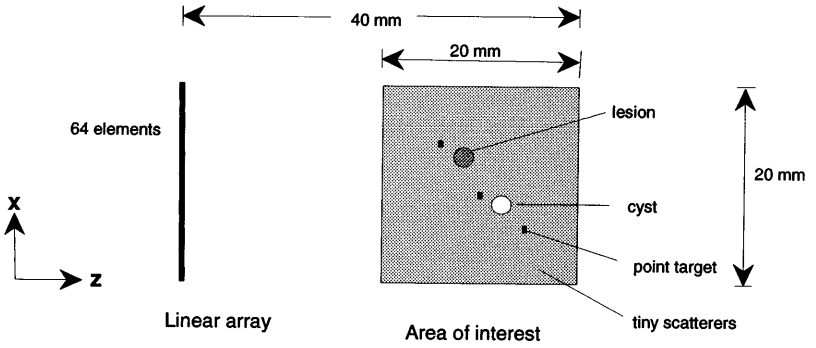

FIG. 4. Geometry of the area of interest.

corresponding subimage elements. For frequency subimage formation, we use different center frequency transmission signals to obtain subimages with different speckle patterns, followed by summation. The correlation coefficient for the two subimages is determined by the difference in the center frequencies and the overlapping bandwidth. We use these subimages to implement the proposed method using simulated images in section 4. The next section gives the details of our method for synthesizing ultrasound images.

3. B-MODE ULTRASOUND IMAGE SIMULATION

There are two classes of theoretical scattering models for ultrasound image formation: the discrete scatterer model and the inhomogeneous continuum model. The discrete scatterer model is widely used for generation of synthetic speckle pattern images [19–22] and is used here. See [23] for a review of the inhomogeneous continuum model. Since the elevation height (about 1 cm) is much larger than the element pitch (about 0.3 mm), a two-dimensional problem is considered.

Figure 4 shows the geometry of the area of interest. x represents the lateral direction of the transducer and z represents its depth. The formulation of an A-line for a phase-sensitive image is

$$B_l(t) = \sum_{j=1}^{N} \sum_{i=1}^{N} \sum_{k=1}^{M} \tau_k P\left(t - \frac{R_{ik}}{c} - \tau_{il} - \frac{R_{jk}}{c} - \tau_{jl}\right), \tag{4}$$

where N is the number of elements, M is the number of scatterers, R_{ik} is the distance between the i^{th} element and the k^{th} scatterer, τ_{il} is the electrical time delay for beamforming (see Section 2), i and j correspond to the transmitting and receiving elements, and $P(t)$ is the pressure pulse. We use a Gaussian shaped pulse as an excitation signal to simplify the frequency-dependent attenuation problem.

For convenience, we rewrite Eq. (4) as follows:

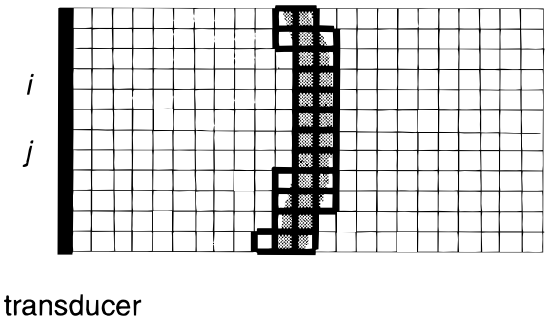

FIG. 5. Insonified scatterers and grids.

$$B_{ij}(t) = \sum_{k=1}^{M} \tau_k P\left(t - \frac{R_{ik}}{c} - \frac{R_{jk}}{c}\right) \tag{5}$$

$$B_l(t) = \sum_{j=1}^{N} \sum_{i=1}^{N} B_{ij}(t - \tau_{il} - \tau_{jl}) \tag{6}$$

Since ultrasonic scatterers in human tissue are dense and randomly distributed in space as well as in reflectivity, computer generation of speckle patterns takes a large amount of computing time if we use Eq. (5) directly (M is often greater than 10,000 for a 2×2 cm^2 area). Hence an efficient method is needed to perform this simulation. In practice, only a small number of scatterers are insonified by a short transmission pulse at any particular time:

$$P(t) \neq 0, \qquad \text{when } 0 \leq t \leq \Delta t \tag{7}$$

The time variable in Eq. (5) is $t - R_{ik}/c - R_{jk}/c$, which should satisfy:

$$0 \leq t - \frac{R_{ik}}{c} - \frac{R_{jk}}{c} \leq \Delta t \Rightarrow ct - c\Delta t \leq R_{ik} + R_{jk} \leq ct \tag{8}$$

This corresponds to scatterers filling in the belt formed by two ellipses (the shadowed part in figure 5). Thus, sorting and grouping scatterers will save significant computing time. On our IBM RISC 6000 system, it takes 3–4 CPU minutes to obtain a single vector B_{ij} in Eq. (5) when scatterers are not sorted and about 20 seconds for sorted scatterers. As shown in figure 5, we divide the area of interest into small cells. Only the scatterers in the cells currently being insonified (highlighted in figure 5) make contributions to $B_{ij}(t)$ at time t.

Synthetic images are thus generated as follows:

Step 1. Generate uniformly distributed scatterers (random positions and reflectivities) and define cysts (containing no scatterers), lesions (with different densities and reflectivities relative to the background), and point targets in the area of interest (Fig. 4).

Step 2. Sort the positions of scatterers along the z (pulse propagation) direction, then group them into small cells (e.g., 1×1 mm^2). Create an information array for the

numbered cells that records the beginning number of the cell in the entire data file. For example, $I(24) = 540$, $I(25) = 587 \cdots$, means that for the 24^{th} cell, the first scatterer parameters are located at the 540^{th} line in the data file and there are 47 scatterers in this cell.

Step 3. Calculate $B_{ij}(t)$ within the insonified cells and record the values for further use.

Step 4. Calculate pixel values using various formulas.
For a phase sensitive image, sum all element signals:

$$B_l(t) = \sum_{j=j_0}^{j_1} \sum_{i=i_0}^{i_1} B_{ij}(t - \tau_{il} - \tau_{jl}). \tag{9}$$

For a power compression image, add power compression and decompression for each element:

$$B_l(t) = \left[\sum_{j=j_0}^{j_1} \left(\sum_{i=i_0}^{i_1} B_{ij}(t - \tau_{il} - \tau_{jl}) \right)^{1/q} \right]^q. \tag{10}$$

Finally, for the spatial subimages needed in the phase insensitive method, sum partial elements to form a subimage:

$$B_l^k(t) = \sum_{j=j_0+h+mn, 0 \le m \le M} \sum_{i=i_0}^{i_1} B_{ij}(t - \tau_{il} - \tau_{jl}). \tag{11}$$

where index l and time t correspond to the position along the transducer direction and axial direction, respectively, and $k = 1, 2, \ldots, n$, (n being the number of subimages). Each transducer has a special value $f_\# = z/L$ that determines the transducer's focusing degree, where z is the depth and L is the effective transducer length. Therefore, the effective transducer length L changes with the depth z and the initial and final indices i_0, j_0 and i_1, j_1, respectively, are dependent on L.

Step 5. Use the Hilbert transform to find the imaginary part of each A-line signal and obtain the envelope of the image.

Step 6. Interpolate or downsample the image to change the number of rows and columns to the desired values. More image lines and a shorter sampling interval give higher image resolution, but the trade-off is much more computing time and greater memory requirements.

4. SIMULATION RESULTS

To obtain a fully developed speckle pattern [5], we chose a scatterer density of 49 mm^{-2} and chose reflectivities randomly from the interval $[-0.1, 0.1]$. In the lesion area, the density was set to 20 mm^{-2} with reflectivities chosen randomly from the interval [0.2, 0.4]. We also placed three point targets in this area with reflectivities of 1 (Fig. 4). The center frequency of the input Gaussian pulse is 5 MHz with a half power bandwidth of

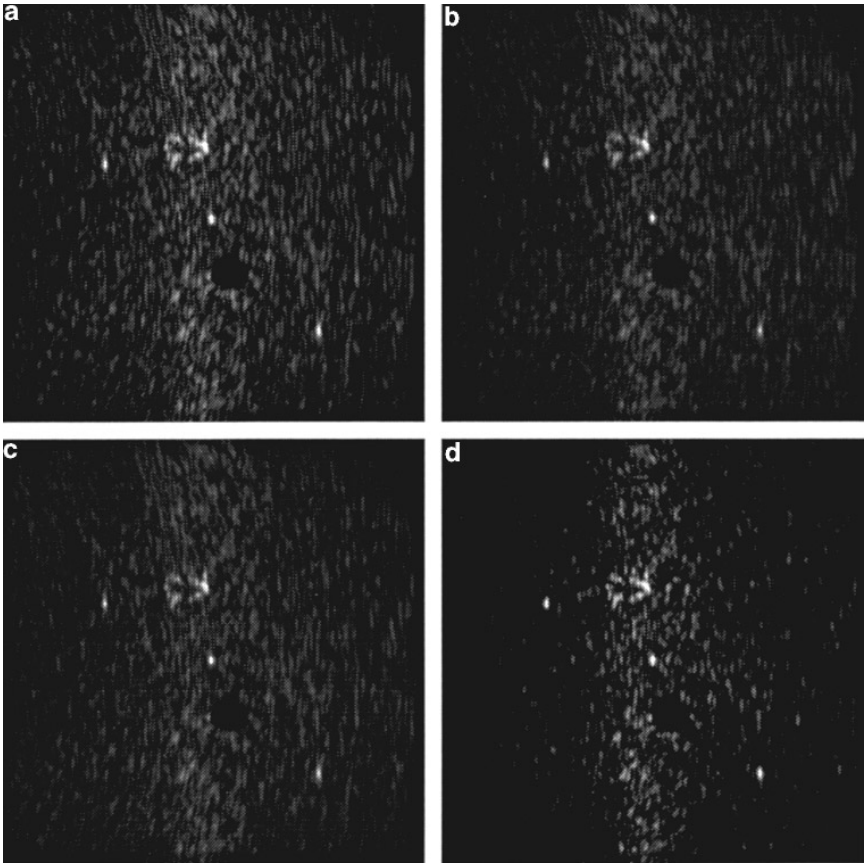

FIG. 6. Original synthetic image and its processed images. (a) (upper left) Original image. (b) (upper right) Spatial homomorphic processing with $n = 2$. (c) (lower left) Frequency homomorphic processing with $n = 2$. (d) (lower right) Power compression with $q = 3$.

1.2 MHz and a sampling frequency of 25 MHz. For the frequency domain filter, $\alpha_1 = 2$, $\alpha_2 = 2$, and the cutoff frequency is 2.8 MHz (relative value: 0.314). We obtain 113 image lines with 675 sample points per line. After resampling, a 337×337 image is obtained.

Images were processed without any intensity transformations; however, to display speckle structure more clearly in the printed figures we transformed the intensities to emphasize moderate and high values. Performance evaluation is based on the original values. Figure 6(a) shows the original phase sensitive image using the fixed focus system given by Eq. (9). From its histogram, we obtain a ratio of sample mean to sample standard deviation in the speckle area of 1.89, which is very close to the expected value of 1.91 [1, 5, 25]. This shows that the speckle pattern of our synthetic image is very close to a Rayleigh distribution.

Figures 6(b) and 6(c) depict results for the spatial and frequency homomorphic processing of figure 6 with $n = 2$ subimages, and $f_1 = 5$ MHz and $f_2 = 4.5$ MHz, respectively. In these images, the noise variance is smaller and features are much clearer than in figure

6. Figure 6(d) shows the results for the power compression method with $q = 3$; speckle is reduced but the edges are blurred as well. In the next section, we discuss the quality and statistics of these images.

5. PERFORMANCE EVALUATION

In this section, we evaluate the performance of our hybrid speckle reduction method. Comparison of images before and after processing is often the best way to evaluate performance. A good image processing technique should reduce speckle noise and preserve interesting features. Usually speckle reduction methods require a trade-off between signal-to-noise ratio and edge resolution. Thus, we need to consider the signal-to-noise ratio in the area of an object to evaluate processing performance.

Our signals are lesion, cyst and point targets. We use an edge detector (discussed later) to find their areas, then obtain their average values and subsequently the variance of the speckle noise.

The contrast-to-noise ratio is defined as:

$$CNR = \frac{\hat{\mu}_s - \hat{\mu}_n}{\hat{\sigma}_n} \tag{12}$$

where $\hat{\mu}_s$ is the mean of the object signal, $\hat{\mu}_n$ is the mean of the speckle noise surrounding the lesion or cyst, and $\hat{\sigma}_n$ is the variance of the speckle noise surrounding the lesion or cyst (the hats denote sample estimators and all values are presented in linear gray level). Contrast refers to the difference between signal and noise.

Another criterion for evaluating image quality is the lesion SNR, defined as:

$$LSNR = \frac{\hat{\mu}_s - \hat{\mu}_n}{(\hat{\sigma}_s^2 + \hat{\sigma}_n^2)^{1/2}} \tag{13}$$

For a cyst, the variance of the signal $\hat{\sigma}_s$ is close to zero so that the CNR and LSNR are virtually the same. For a lesion, we assume the speckle smoothing algorithm does not increase the variance of the signal near the lesion. In most cases, the variance is actually reduced. Consequently, the improvement in the LSNR is larger than in the CNR when the original and processed images are compared. Because we are more interested in speckle reduction and contrast improvement, we use the contrast-to-noise ratio and edge detection quality to test the performance of our method.

Figures 7 and 8 show that the CNR of the synthetic images changes with processing methods. The starting values represent the CNRs of the original image in the lesion, cyst or point target areas (see the “region” definition in the next paragraphs). The proposed spatial homomorphic method improves the CNR about 25% for point targets and lesions. The frequency homomorphic method performs better for cyst detection (increasing the CNR by 15%). This is because in our experiment the correlation coefficient of the subimages for frequency homomorphic processing is smaller than that for spatial homomorphic processing. The small correlation coefficient is good for noise reduction but also obscures point targets, as discussed earlier. In our experiments, increasing the number of

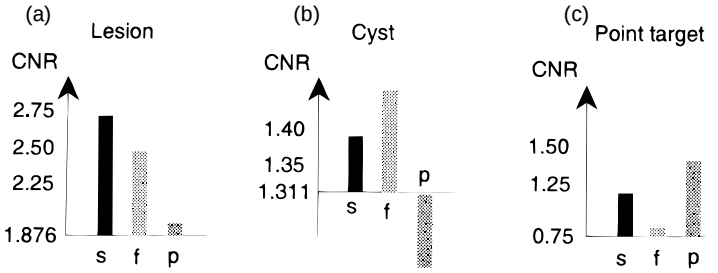

FIG. 7. Contrast-to-noise ratio (CNR) in point, lesion and cyst areas. The starting values represent the corresponding CNRs in the original image. s = spatial homomorphic, f = frequency homomorphic, p = power compression. (a) lesion, (b) cyst, (c) point target.

subimages improves the CNR slightly, 4% in lesion areas and 20% in point target areas. Only for point target detection does power compression perform as well as the proposed homomorphic method.

Normal edge detection methods require that the regions of interest be homogeneous. The granular structure of speckle in ultrasound images makes normal edge detection inappropriate [24]. The following is a specialized edge detection technique for use with images containing speckle patterns.

At the edge of a lesion or a cyst, the pixel values change greatly. We set two thresholds, one a gradient type T_g and the other a ratio type T_r. The gradient magnitude at (i, j) is approximated by

$$g(i, j) = |P(i, j) - P(i, j + 1)| + |P(i, j) - P(i + 1, j)| \tag{14}$$

and the contrast ratio at (i, j) is defined by

$$r(i, j) = max\left[\frac{P(i, j)}{P(i, j + 1)}, \frac{P(i, j + 1)}{P(i, j)}, \frac{P(i, j)}{P(i + 1, j)}, \frac{P(i + 1, j)}{P(i, j)}\right] \tag{15}$$

where $P(i, j)$ is the pixel value at (i, j). If $g(i, j) > T_g$ or $r(i, j) > T_r$, (i, j) is labeled as an edge pixel.

We check the edge points line by line in the lesion or cyst window and locate the first and last edge points for each line. We then connect these points to their neighbors on adjacent scan lines. The area enclosed gives the size of a lesion or cyst.

In this section, the area size and CNR are based on edge detection which is clearly affected by the threshold selection. Setting a reasonable threshold is very important to performance evaluation. After checking the highlighted edges in the original image, we determine reasonable thresholds and sizes of lesions and cysts and try several thresholds for each processed image to select the same sizes of lesions and cysts as the original. This technique allows comparison of edge preservation and localization for the same conditions.

After several experiments, we obtain the thresholds associated with each type of processing. Changing these thresholds by a specified amount causes a change in the estimated area of the region. If the change in the area for a processed image is much larger than

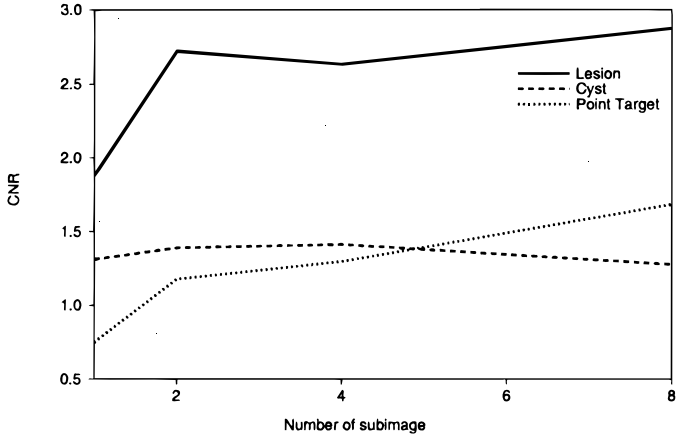

FIG. 8. CNR versus number of subimages in spatial homomorphic imaging. (Solid line = lesion, dashed line = cyst, dotted line = point target.)

for the original one, it means the edge is blurred during the processing. In our experiments, we set a change in threshold of Δ, which corresponds to about a 5% decrease in the lesion (or cyst) size in the original image, then use this Δ to find the lesion (or cyst) size changes for the other types of processing. Figure 9 shows the results. As can be seen, power compression processing causes significant blurring of the edges of a cyst.

Preservation of lesion and cyst size with processing does not guarantee preservation of location. Thus, we must also verify localization.

For a detected signal (lesion or cyst), we define its centroid (x_c, z_c):

$$x_c = \frac{1}{P} \sum_{i=1}^{P} x_i \tag{16}$$

$$z_c = \frac{1}{P} \sum_{i=1}^{P} z_i \tag{17}$$

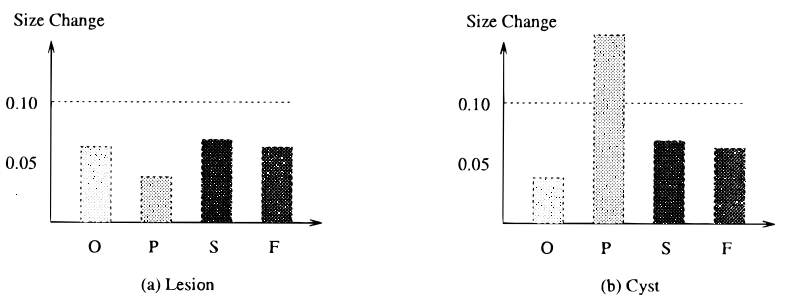

FIG. 9. The change in size of a lesion and cyst for a specific threshold change.

TABLE 1
Centroid Distance and Overlap Degree for Lesion and Cyst with Different Processing

Method	Lesion D_c (mm)	Lesion O_d %	Cyst D_c (mm)	Cyst O_d %
original	0.000	100	0.000	100.
power(n = 3)	0.1317	86.2	0.1387	87.3
spat. homo.(n = 2)	0.0768	92.3	0.0796	94.0
spat. homo.(n = 4)	0.1305	87.2	0.0368	95.8
freq. homo.(n = 2)	0.0760	92.5	0.0387	97.2

Note. 1 mm $\approx$ 16.8 pixels.

where P is the total number of pixels included in the area. For the centroid of a signal in the original image (x_1, z_1) and the centroid of the same signal in the processed image (x_2, z_2), we define the distance between centroids D_c by

$$D_c = \sqrt{(x_1 - x_2)^2 + (z_1 - z_2)^2} \tag{18}$$

We compare the same signal in both the original and processed images and divide its area into overlap and uncovered parts. The degree of overlap O_d is given by

$$O_d = \frac{M}{P} \tag{19}$$

where M is the number of pixels in the overlap area.

Tables 1 and 2 give the distances between centroids and the degrees of overlap. In our experiments, both spatial and frequency homomorphic processing preserve signal location, but power compression processing does not. Since overlap is a function of both shrinkage/dilation and centroid motion, table 1 shows that centroid motion is a major component of the overlap decrease in our experiments.

6. PARAMETER TESTING

The parameters used for both the subimages and low pass filter affect image feature detection. In this section, we show the relationship between the correlation coefficients for the subimages and the CNRs and also test the parameters used for the low frequency emphasis filter.

TABLE 2
Centroid Distance and Overlap Degree for Cyst and Point Target with Different Processing

Method	Cyst distance pixels	Cyst overlap %	Point distance pixels	Point overlap. %
original	0.00	100.0	0.00	100.0
homo.(n = 2)	4.23	96.02	0.167	94.4
homo.(n = 4)	0.84	95.22	0.167	94.4
homo.(n = 8)	4.73	98.16	0.167	94.4
power(q = 3)	3.87	90.14	0.304	95.24

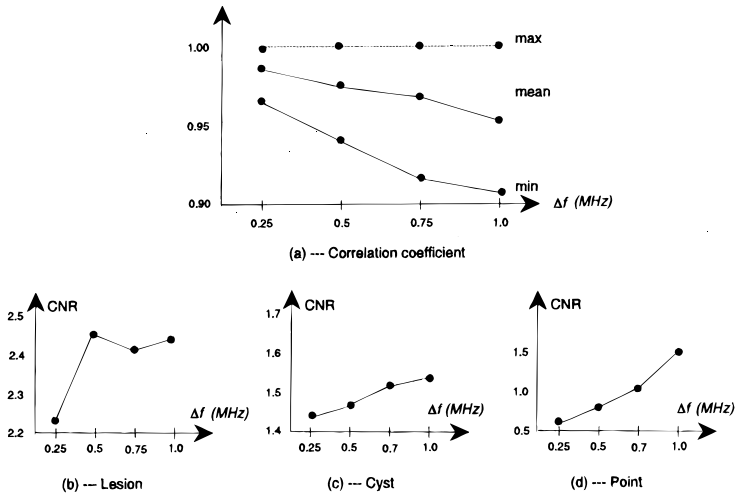

FIG. 10. Correlation coefficients and CNRs for lesion, cyst and point target.

Using frequency homomorphic processing with $n = 2$, we increase the frequency difference Δf by increments of 0.25 MHz. Figure 10(a) shows the correlation coefficients for the subimages. Figures 10(b)–(d) give the CNRs for a lesion, cyst and point target as a function of Δf. The results agree with the discussion in section 2: As the frequency difference is increased, the correlation coefficient for the subimages becomes smaller and both the signal and noise levels decrease. The CNR has a maximum value for a lesion signal. For a cyst and point target, the CNR increases with Δf.

The low frequency emphasis filter is of major importance in our algorithm. Figures 11 and 12 depict the changes in the CNR as a function of the cutoff frequency and as a function of $\alpha(\alpha = \alpha_1 = \alpha_2)$, respectively. Figure 11 shows that as the cutoff frequency f_c is increased, the CNR for a point target increases and the CNRs for a lesion and cyst have a peak at $f_c = 0.2$ (relative value). This is because in the frequency domain, point targets correspond to high frequency components, cysts to low frequency components, and lesions (as concentrated discrete scatterers) have a frequency component band in between that of point targets and cysts.

Figure 12 indicates that a high α is good for lesion and point detection but not for cyst detection. From our algorithm, we know that α is an exponential coefficient, which

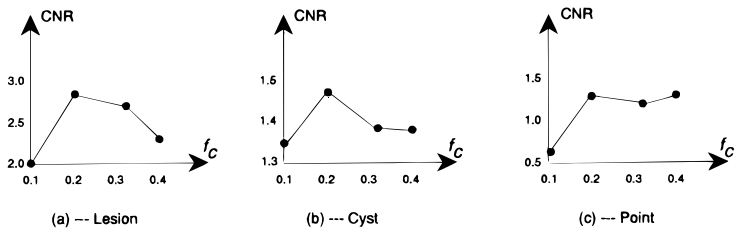

FIG. 11. CNR with cutoff frequency changes.

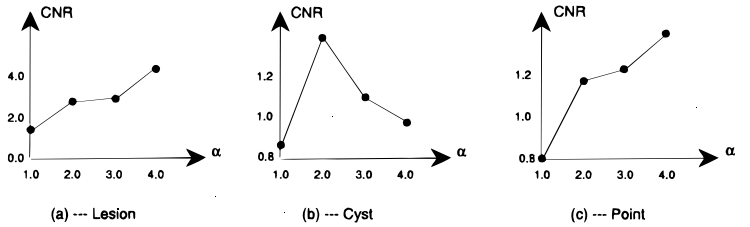

FIG. 12. CNR with constant α.

stretches the gray level exponentially. To optimize detection for all three targets, we choose $\alpha = 2$ and $f_c = 0.314$ (relative value) for our experiments.

7. REAL IMAGE TESTING

Results for the hybrid homomorphic imaging technique were compared with real image results for a phantom. The phantom, constructed with a void to model a cyst and several point targets, was scanned and 128 channel signals were recorded individually. Each image frame consists of 192 image lines and 658 samples per line. The transducer center frequency is 5MHz and its bandwidth is 3.8MHz.

Figure 13(a) shows the original image, and figures 13(b) and 13(c) show the processing results for the phase insensitive homomorphic method. The point targets are clear in all three images. The cyst is hard to find in the original image, but it is clear in figures 13(b) and 13(c).

Figure 13(d) depicts the power compression results for the original image. It is obvious that the CNR in the cyst area is not improved and it is difficult to distinguish point targets from speckle noise.

The CNRs (Fig. 14) give more details in the area of the objects. The phase insensitive homomorphic method improves the CNRs significantly for both cysts and point targets. The optimal number of subimages is either 2 or 4. When a larger number of subimages is used, the image becomes smoother, causing difficulties with edge detection and decreasing the CNR for a cyst. The small number of subimages required has the advantage of making it easy to implement this method in a real ultrasound device.

Table 2 gives the location properties for the cyst and point targets for different processing. The high overlap rates and small distances between centroids show that the nonlinear phase insensitive method does not cause distortion.

The parameters used in the experiments above are: $\alpha_1 = 2$, $\alpha_2 = 2$, and f_c (cutoff frequency) $= 0.2$. These values were found to be optimal empirically.

8. CONCLUSIONS

In this paper we have presented a new method for speckle reduction. Phase insensitive homomorphic processing is a hybrid method. It combines the noise immunity of phase sensitive imaging and the high resolution of image multiplication. The combination of

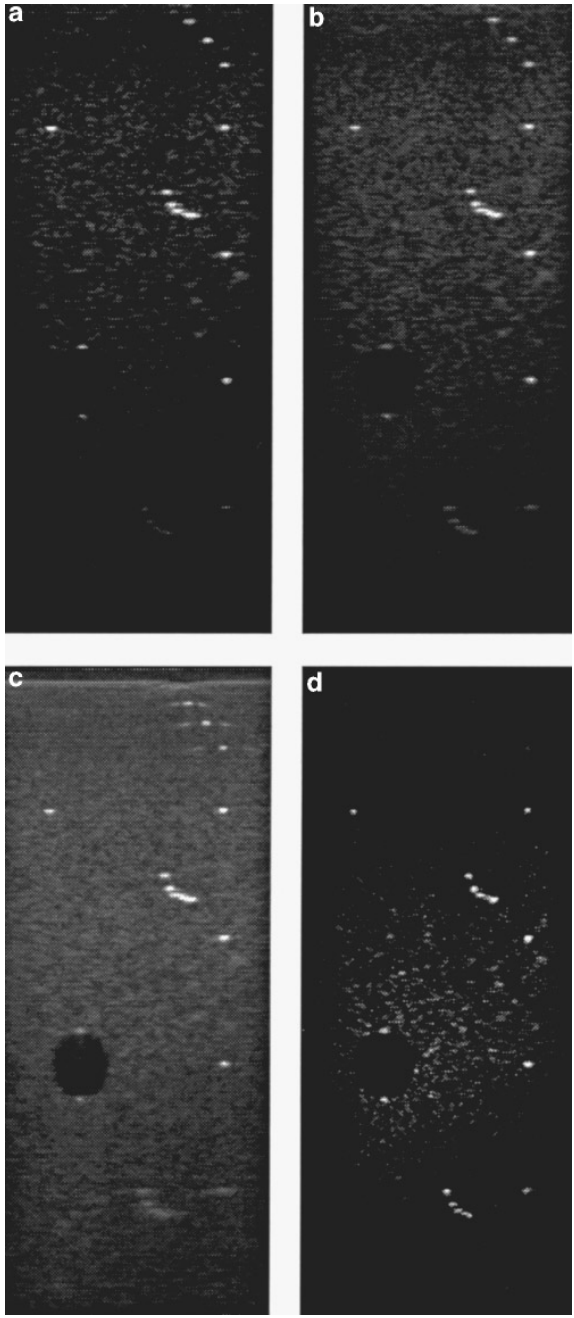

FIG. 13. Original real image and its processed images. (a) (upper left) Original image. (b) (upper right) Spatial homomorphic processing with $n = 2$. (c) (lower left) Spatial homomorphic processing with $n = 4$. (d) (lower right) Power compression with $q = 3$.

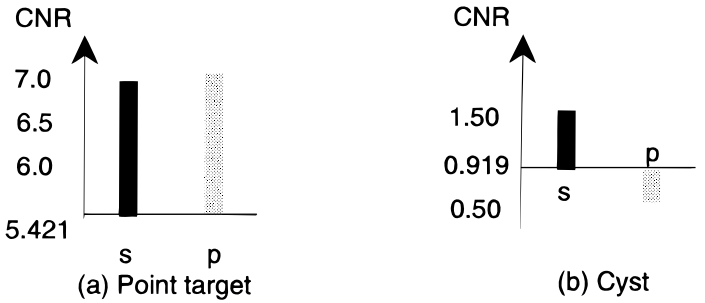

FIG. 14. CNR in real image. The starting values represent the corresponding CNRs in the original image. s = spatial homomorphic, p = power compression. (a) point target, (b) cyst.

four factors (correlated image multiplication, dynamic range compression, low frequency emphasis filter and scale enlargement) works well in speckle noise reduction. The contrast-to-noise ratio improves greatly: Spatial subimaging works well in lesion and point target areas while frequency subimage processing is better for cyst detection. The other benefit of this method is that it preserves edge features. The final image can be controlled by changing filter parameters to obtain a better image with low speckle noise and distinguishable lesions, cysts and point targets.

ACKNOWLEDGMENTS

This work was supported by the National Science Foundation under grant ECS-9253547 and by the Carl M. Hansen Foundation.

REFERENCES

[1] Burckhardt, C. B., Speckle in ultrasound B-Mode scans, *IEEE Trans. Sonics Ultrasonics, SU-25*, 1–6 (1978).

[2] Flax, S. W., Glover, G. H., and Pelc, N. J., Textural variations in B-mode ultrasonography: A stochastic model, *Ultrasonic Imaging 3*, 235–257 (1981).

[3] Abbott, J. G., and Thurstone, F. L., Acoustic speckle: Theory and experimental analysis, *Ultrasonic Imaging 1*, 303–324 (1979).

[4] Dainty, J. C., *Laser Speckle and Related Phenomena*, 9–75 (Springer–Verlag, Berlin/Heidelberg/NY, 1975).

[5] Tuthill, T. A., Sperry, R. H., and Parker, K. J., Deviations from Rayleigh statistics in ultrasonic speckle, *Ultrasonic Imaging 10*, 81–89 (1988).

[6] Goodman, J. W., A random walk through the field of speckle, *Optical Engin. 25*, 610–612 (1986).

[7] Wagner, R. F., Insana, M. F., and Brown, D. G., Statistical properties of radio-frequency and envelope-detected signals with applications to medical ultrasound, *J. Opt. Soc. Am. 4*, 910–922 (1986).

[8] Magnin, P. A., von Ramm, O. T., and Thurstone, F. L., Frequency compounding for speckle contrast reduction in phased array images, *Ultrasonic Imaging 4*, 267–281 (1982).

[9] Galloway, R. L., McDermott, B. A., and Thurstone, F. L., A frequency diversity process for speckle reduction in real-time ultrasonic images, *IEEE Trans. Ultrason. Ferroelec. Freq. Contr., 35*, 45–49 (1988).

[10] Giesey, J. J., Carson, P. L., Fitting, D. W., and Meyer, C. R., Speckle reduction in pulse-echo ultrasonic

imaging using a two-dimensional receiving array, *IEEE Trans. Ultrason. Ferroelec. Freq. Contr., 39*, 167–173 (1992).

[11] Trahey, G. E., Smith, S. W., and Von Ramm, O. T., Speckle pattern correlation with lateral aperture translation: experimental results and implications for spatial compounding, *IEEE Trans. Ultrason. Ferroelec. Freq. Contr., 33*, 257–264 (1986).

[12] Loupas, T., McDicken, W. N., and Allan, P. L., Adaptive weighted median filter for speckle suppression in medical ultrasonic images, *IEEE Trans. Circuits and Systems 36*, 129–135 (1989).

[13] Bamber, J. C., and Daft, C., Adaptive filtering for reduction of speckle in ultrasonic pulse-echo images, *Ultrasonics 24*, 41–44 (1986).

[14] Crimmins, T. R., Geometric filter for speckle reduction, *Applied Optics 24*, 1438–1443 (1985).

[15] Fong, Y. S., Pomalaza-Raez, C. A., and Wang, X. H., Comparison study of nonlinear filters in image processing applications, *Optical Engin. 28*, 749–760 (1989).

[16] Kotropoulos, C., and Pitas, I., Optimum nonlinear signal detection and estimation in the presence of the ultrasonic speckle, *Ultrasonic Imaging 14*, 249–275 (1992).

[17] O'Donnell, M., Phase-insensitive pulse-echo imaging, *Ultrasonic Imaging 4*, 321–335 (1982).

[18] Laugier, P., Fink, M., and Abouelkaram, S., The random phase transducer: a new technique for incoherent processing-experimental results, *IEEE Trans. Ultrason. Ferroelec. Freq. Contr., 37*, 70–78 (1990).

[19] Foster, D. R., Arditi, M., Foster, F. S., Patterson, M. S., and Hunt, J. W., Computer simulation of speckle in B-scan images, *Ultrasonic Imaging 5*, 308–330 (1983).

[20] Oosterveld, B. J., Thijseen, J. M., and Verhoef, W. A., Texture of B-mode echograms: 3-D simulations and experiments of the effects of diffraction and scatterer density, *Ultrasonic Imaging 7*, 142–160 (1985).

[21] Bamber, J. C., and Dickinson, R. J., Ultrasonic B-scanning: a computer simulation, *Phys. Med. Biol. 25*, 463–479 (1980).

[22] Park, J. C., and Park, S. B., An efficient computer model of three-dimensional speckle patterns in dynamically focused annular array, *Ultrasonic Imaging 15*, 103–121 (1993).

[23] Dickinson, R. J., A computer model for speckle in ultrasound images: theory and application, *Acoustical Imaging 10*, 115–129, A. F. Metherell, Ed., (New York, 1982).

[24] Czerwinski, R. N., Jones, D. L., and O'Brien, W. D., Jr., Edge detection in ultrasound speckle noise, *IEEE Proceed. ICIP I*, 304–308 (1994).

[25] Wagner, R. F., Smith, S. W., Sandrik, J. M., and Lopez, H., Statistics of speckle in Ultrasound B-scans, *IEEE Trans. Sonics Ultrasonics SU-30*, 156–163 (1983).